Pharm Res (2014) 31:2203–2219
DOI 10.1007/s11095-014-1319-1

RESEARCH PAPER

Mechanistic Understanding of Brain Drug Disposition to Optimize the Selection of Potential Neurotherapeutics in Drug Discovery

Irena Loryan • Vikash Sinha • Claire Mackie • Achiel Van Peer • Wilhelmus Drinkenburg • An Vermeulen • Denise Morrison • Mario Monshouwer • Donald Heald • Margareta Hammarlund-Udenaes

Received: 9 September 2013 / Accepted: 28 January 2014 / Published online: 13 March 2014

ABSTRACT

Purpose The current project was undertaken with the aim to propose and test an in-depth integrative analysis of neuropharmacokinetic (neuroPK) properties of new chemical entities (NCEs), thereby optimizing the routine of evaluation and selection of novel neurotherapeutics.

Methods Forty compounds covering a wide range of physicochemical properties and various CNS targets were investigated. The combinatory mapping approach was used for the assessment of the extent of blood-brain and cellular barriers transport via estimation of unbound-compound brain ($K_{p,uu,brain}$) and cell ($K_{p,uu,cell}$) partitioning coefficients. Intra-brain distribution was evaluated using the brain slice method. Intra- and sub-cellular distribution was estimated via calculation of unbound-drug cytosolic and lysosomal partitioning coefficients.

Results Assessment of $K_{p,uu,brain}$ revealed extensive variability in the brain penetration properties across compounds, with a prevalence of compounds actively effluxed at the blood-brain barrier. $K_{p,uu,cell}$ was valuable for identification of compounds with a tendency to accumulate intracellularly. Prediction of cytosolic and lysosomal partitioning provided insight into the subcellular accumulation. Integration of the neuroPK parameters with pharmacodynamic readouts demonstrated the value of the proposed approach in the evaluation of target engagement and NCE selection.

Conclusions With the rather easily-performed combinatory mapping approach, it was possible to provide quantitative information supporting the decision making in the drug discovery setting.

KEY WORDS blood-brain barrier · brain drug delivery · neuropharmacokinetics · neurotherapeutics · screening cascade · unbound-drug

ABBREVIATIONS

A_{brain}	Amount of drug in brain tissue
AUC_{0-t}	Area under the drug concentration-time curve from zero to t, where t is the last time point with a measurable concentration for an individual dose

Electronic supplementary material The online version of this article (doi:10.1007/s11095-014-1319-1) contains supplementary material, which is available to authorized users.

I. Loryan • M. Hammarlund-Udenaes (✉)
Translational PKPD Group, Department of Pharmaceutical Biosciences
Associate Member of SciLife Lab, Uppsala University, Box 591, 751 24 Uppsala, Sweden
e-mail: mhu@farmbio.uu.se

V. Sinha • A. Van Peer
Clinical Pharmacology, Janssen Research and Development, A Division of Janssen Pharmaceutica NV, Beerse, Belgium

C. Mackie
Pharmaceutical Development and Manufacturing Science
Janssen Research and Development, A Division of Janssen Pharmaceutica NV, Beerse, Belgium

W. Drinkenburg
Neuroscience Discovery, Janssen Research and Development
A Division of Janssen Pharmaceutica NV, Beerse, Belgium

A. Vermeulen
Model Based Drug Development, Janssen Research & Development
A Division of Janssen Pharmaceutica NV, Beerse, Belgium

D. Morrison
Early Drug Developability Group
CREATe (Community for Research Excellence and Advanced Technologies), Janssen Research and Development, A Division of Janssen Pharmaceutica NV, Beerse, Belgium

M. Monshouwer
BA/DMPK, Janssen Research and Development
A Division of Janssen Pharmaceutica NV, Beerse, Belgium

D. Heald
Clinical Pharmacology, Janssen Research & Development, LLC
Titusville, Florida, USA

$AUC_{tot,brain}$	Area under the total drug brain concentration-time curve
$AUC_{tot,plasma}$	Area under the total drug plasma concentration-time curve
BBB	Blood-brain barrier
BCRP	Breast cancer resistance-associated protein
BCSFB	Blood-CSF barrier
CB	Cellular barrier
C_{buffer}	Concentration of compound in the buffer (brain slice method)
CNS	Central nervous system
CSF	Cerebrospinal fluid
$C_{tot,brain}$	Total drug concentration in brain
$C_{tot,plasma}$	Total drug concentration in plasma
$C_{u,brainISF}$	Unbound-drug concentration in brain interstitial fluid
$C_{u,plasma}$	Unbound-drug concentration in plasma
ECF	Extracellular fluid (same as ISF)
ED	Equilibrium dialysis
$f_{u,brain}$	Unbound fraction of drug in brain homogenate
$f_{u,brain,corrected}$	Unbound fraction of drug in brain homogenate after applying the correction using the pH partitioning model
$f_{u,hD}$	Unbound fraction of drug in diluted brain homogenate
$f_{u,plasma}$	Unbound fraction of drug in plasma
ICF	Intracellular fluid in the brain
ISF	Interstitial fluid in the brain (same as ECF)
$K_{p,brain}$	Ratio of total brain to total plasma drug concentrations (general annotation)
$K_{p,brainSD}$	Ratio of total brain to total plasma drug concentrations measured after single dose administration
$K_{p,brainSS}$	Ratio of total brain to total plasma drug concentrations at steady-state
$K_{p,CSF}$	Ratio of total plasma to total CSF drug concentrations
$K_{p,uu,brain}$	Ratio of brain ISF to plasma unbound-drug concentrations
$K_{p,uu,cell}$	Ratio of brain ICF to ISF unbound-drug concentrations
$K_{p,uu,cell,obs}$	$K_{p,uu,cell}$ determined using the combination of brain slice and brain homogenate methods
$K_{p,uu,cell,pred}$	$K_{p,uu,cell}$ predicted using the three-compartment pH partitioning model
$K_{p,uu,CSF}$	Ratio of plasma to CSF unbound-drug concentrations
$K_{p,uu,cyto,pred}$	Ratio of cytosolic to extracellular unbound-drug concentrations predicted from the pH partitioning model
$K_{p,uu,lyso,pred}$	Ratio of lysosomic to cytosolic unbound-drug concentrations predicted from the pH partitioning model
LC-MS/MS	Liquid chromatography tandem mass spectrometry
NCE	New chemical entity
neuroPK	Neuropharmacokinetics
P-gp	P-glycoprotein
$V_{u,brain}$	Volume of distribution of unbound-drug in brain ($mL \cdot g\ brain^{-1}$)

INTRODUCTION

The need for innovative new medicines for the treatment of chronic mental disorders and neurodegenerative diseases is currently imperative; and is far beyond the scope of only the pharmaceutical industry. The fact that out of 259 new chemical entities (NCEs) and biologics approved by the US Food and Drug Administration between 1999 and 2008 only eight small molecules were first-in-class CNS drugs, provides the greatest evidence of the worrisome trend in CNS drug discovery (1). In contrast, thousands of compounds are screened on a yearly basis in an attempt to identify potential novel CNS drug candidates. The causes for the higher attrition rates in the CNS compared to other therapeutic areas have been scrutinized from different perspectives and numerous pharmacodynamic (PD), pharmacokinetic (PK) and translational reasons have been acknowledged (2–7).

According to the current perception of brain PK, pharmacologically, a sufficient exposure of drug at the target-site over a desired period of time is pivotal for CNS drug action and is a prerequisite for advancement of NCEs within the CNS area (2,8–11). Furthermore, based on extensive PKPD studies of marketed CNS drugs, it has become abundantly clear that the brain interstitial fluid (ISF) concentration, which is in essence the concentration of unbound-drug ($C_{u,brainISF}$), is an appropriate measure of CNS exposure for extracellular pharmacological targets (2,9,12–18). However, direct assessment of unbound-drug CNS exposure is often not attainable experimentally or clinically. Moreover, the presence of the blood-brain barrier (BBB) often leads to asymmetry in drug BBB transport which does not allow the use of plasma unbound-drug concentration as a surrogate of intracerebral target-site drug concentration (9). To take the quantitative influence of active efflux or influx at the BBB into consideration, the ratio of brain ISF to plasma unbound-drug concentrations needs to be assessed (9,14). This is denoted $K_{p,uu,brain}$ and designates the net flux of drug across the BBB.

$K_{p,uu,brain}$ can be estimated using a combinatory approach based on steady-state total brain ($C_{tot,brain}$) and total plasma concentrations ($C_{tot,plasma}$), corrected for the unbound fraction of the compound in brain homogenate ($f_{u,brain}$) and plasma ($f_{u,plasma}$) (13,17,19–22). With the development of the high-throughput brain slice method, intended for the assessment of

overall brain tissue binding and distribution of compounds via the volume of distribution of unbound-drug in brain ($V_{u,brain}$), it has become possible to evaluate $K_{p,uu,brain}$ more accurately (22–24).

Another challenging step in neuropharmacokinetics (neuroPK) is to improve the understanding of not only the BBB transport of NCEs but also the intra- and sub-cellular distribution of compounds, which has to be evaluated in a pharmacodynamic context for intracellular pharmacological target(s). In this regard, estimation of the unbound-drug cell partitioning coefficient $K_{p,uu,cell}$ is a unique and innovative approach, accomplished by a combination of the brain slice and brain homogenate techniques (13). Additionally, prediction of intracellular sequestration of the compounds, e.g. accumulation of bases in the acidic organelles, provides further insight to target-site pharmaco- and toxicokinetics (25).

In spite of the progress made in understanding BBB transport, the integrative quantitative assessment of the myriad of processes, involved in the brain disposition of NCEs, is still highly inadequate and often marginalized in drug discovery programs.

Therefore, the current project was undertaken with the intent to propose and assess an integrative analysis of neuroPK properties of NCEs, with the aim of optimizing the routine evaluation and selection of neurotherapeutics using this novel procedure. With this objective in mind, we have investigated and compared 40 compounds regarding their neuroPK properties, in particular the extent of BBB transport ($K_{p,uu,brain}$), the intra-brain distribution ($V_{u,brain}$), the cellular barrier transport ($K_{p,uu,cell}$) as well as the intracellular distribution into the cytosol and acidic organelles ($K_{p,uu,cyto,pred}$ and $K_{p,uu,lyso,pred}$, respectively).

MATERIALS AND METHODS

Experimental Procedures

Selection of Compounds

A novel dataset comprising of 40 compounds covering a wide range of physicochemical properties and various pharmacological CNS targets was assembled. Compounds were assigned to nine groups based on the pharmacological targets (Table I).

Group A and B are inhibitors of phosphodiesterase 10 (PDE10) and 2 (PDE2). Group C consists of gamma secretase (GS) modulators. Group D and E are positive allosteric modulators of metabotropic glutamate receptor 2 ($mGlu_2$) and 5 ($mGlu_5$). Group F consists of positive allosteric modulator of nicotinic alpha 7 receptor (alpha 7), antagonists of dopamine D_2/D_3 and 5-hydroxytryptamine 5HT6/5HT2/5HT2A receptors. Group G is composed of inhibitors of beta-site amyloid precursor protein cleaving enzyme (BACE). Group H consists of antagonists of the histamine H4 receptor. Group I is composed of antagonists of P2X purinoceptor 7 (P2X7).

Thirty three compounds were obtained from the Janssen Research and Development in-house compound library (Beerse, Belgium and La Jolla, USA). Four compounds were selected from pharmacological analogues developed at Bayer AG (B5 – Bay 60–7550, (26)), Novartis International AG (G10 – 5-Cyano-pyridine-2-carboxylic acid [3-(5-amino-3-difluoromethyl-3,6-dihydro-2H-[1,4]oxazin-3-yl)-phenyl]-amide) and Eli Lilly&Co (G6 – LY2811376, (27), G9 – LY2886721 with Clinical Trials Identifier: NCT01561430). Three post-marketing antipsychotics risperidone (F4), paliperidone (F5) and olanzapine (F6) were also incorporated in the dataset. The majority of the compounds (24) were in the preclinical stage at the moment of inclusion. As the current dataset was comprised mainly of potential CNS drug candidates, apart from H1 and H2, it was biased with regard to the ion class representation, i.e. 30 compounds were bases. The purity of all batches used in this study was evaluated to be equal to or greater than 95% using standard in-house analytical methods.

Animals

Drug-naïve male Sprague Dawley 250–300 g rats (Taconic, Lille Skensved, Denmark) were used for preparation of fresh brain slices. All animals were housed in groups at 18 to 22°C under a 12-h light/dark cycle with *ad libitum* access to food and water. The brain slice *in vitro* experiments were approved by the Animal Ethics Committee of Uppsala, Sweden (Ethical Approval N° C329/10 and C351/11). Male Sprague Dawley rats and Swiss SPF mice obtained from Charles River Laboratories, Inc. (Germany) were used in *in vivo* pharmacokinetic studies conducted at Janssen R&D.

The Brain Slice Method

Herein, we have chosen to express information from brain slice studies as $V_{u,brain}$ and information from the brain homogenate binding studies as $f_{u,brain}$ to differentiate and clarify the source of the information as much as possible.

The volume of distribution of unbound-compound in brain ($V_{u,brain}$) was estimated for the compounds using the brain slice method according to previously published protocols (23,24). Briefly, six 300 μm brain slices obtained using a vibrating blade microtome Leica VT1200 (Leica Microsystems AB, Sweden) were incubated in a HEPES-buffered artificial extracellular fluid (aECF) containing a mixture of five compounds (termed "cassette") with an initial concentration of 200 nM of each compound. The formation of cassettes was based on

Table I Pharmacological Target(s), Ion Class, Molecular Weight (MW), Octanol-Water Partitioning Coefficient (logP) and Dissociation Constant/s (pKa) of 40 Structurally Diverse Compounds

ID	Pharmacological target	Ion class	MW	logP	Measured pKa[a]
A1	PDE10	Weak base	353.4	2.4	4.4/2.6
A2	PDE10	Weak base	379.5	2.6	4.4/3.1
A3	PDE10	Weak base	369.4	1.6	3.87/2.27
B1	PDE2	Weak base	362.3	3.9	4.0
B2	PDE2	Weak base	432.5	2.6	5.6/1.9
B3	PDE2	Neutral	397.4	1.8	NMIG
B4	PDE2	Weak base	412.4	1.4	2.8
B5 [R1]	PDE2	Weak base	476.6	*N.A.*	9.4/3.4
C1	GS	Weak base	447.4	4.2	5.7
C2	GS	Base	454.5	4.0	6.0
C3	GS	Weak base	417.3	3.3	5.6
D1	$mGlu_2$	Neutral	344.9	4.6	NMIG
D2	$mGlu_2$	Weak base	451.4	4.2	5.0
D3	$mGlu_2$	Base	454.4	4.3	6.3
D4	$mGlu_2$	Neutral	380.9	>5	NMIG
E1	$mGlu_5$	Neutral	338.3	2.8	NMIG
E2	$mGlu_5$	Neutral	352.4	3.1	NMIG
F1	alpha 7	Weak base	416.4	3.1	3.5
F2	fast D_2	Base	372.3	4.0	7.76/2.12
F3	D_2/D_3/5HT6	Base	308.3	2.6	8.2
F4[b]	D_2/5HT2	Base	410.5	3.0	8.24/3.11
F5[b]	D_2/5HT2	Base	426.5	2.4	8.2/2.6
F6[b]	D_2/5HT2A	Base	312.4	2.8	8/5.6
G1	BACE	Base	377.4	1.9	7.8
G2	BACE	Base	427.4	2.4	7.9
G3	BACE	Base	445.4	2.8	7.5
G4	BACE	Base	389.4	1.0	8.2
G5	BACE	Base	378.9	1.6	9.2
G6[R2]	BACE	Base	320.4	1.0	8.5
G7	BACE	Base	421.4	2.7	7.8
G8	BACE	Base	371.3	2.2	7.9
G9[R3]	BACE	Base	390.4	2.4	7.7
G10[R4]	BACE	Base	389.3	1.9	7.4
H1	H4	Base	263.3	−0.83	8.58/5.91
H2	H4	Base	233.3	0.3	8.69/6.32
I1	P2X7	Neutral	375.2	1.4	NMIG
I2	P2X7	Neutral	405.8	2.4	NMIG
I3	P2X7	Neutral	374.2	2.4	NMIG
I4	P2X7	Neutral	388.3	2.0	NMIG
I5	P2X7	Neutral	421.8	2.8	NMIG

Group A: inhibitors of PDE10 (Phosphodiesterase 10); Group B: inhibitors of PDE2 (Phosphodiesterase 2); Group C: modulators of GS (Gamma secretase); Group D: positive allosteric modulators of $mGlu_2$ receptor (Metabotropic glutamate receptor 2); Group E: positive allosteric modulators of $mGlu_5$ receptor (Metabotropic glutamate receptor 5); Group F: positive allosteric modulator of nicotinic alpha 7 receptor (alpha 7 nicotinic receptor); antagonists of D_2/D_3 (dopamine D_2/D_3 receptors), and antagonists of 5HT6/5HT2/5HT2A (5-hydroxytryptamine 5HT6/5HT2/5HT2A receptors); Group G: inhibitors of BACE (beta-site amyloid precursor protein cleaving enzyme); Group H: antagonists of H4 receptor (histamine H4 receptor); Group I: antagonists of P2X7 receptor (P2X purinoceptor 7).

N.A. not available; NMIG no measurable ionisable groups (pKa equal or lower than 2)

[a] The dissociation constant was determined at 25°C by potentiometric titration of a solution of the compounds using Sirius T3 instrument (Sirius Analytical Ltd., UK)

[b] F4 – risperidone, F5 – paliperidone, F6 – olanzapine

[R1] - Bayer AG (BAY60-7550), [R2] - Eli Lilly (LY2811376), [R3] - Eli Lilly&Co (LY2886721), [R4] - Novartis International AG (5-Cyano-pyridine-2-carboxylic acid [3-(5-amino-3-difluoromethyl-3,6-dihydro-2H-[1,4]oxazin-3-yl)-phenyl]-amide)

compatibility of the bioanalytical methods (see, Supplementary Material, Table SI for arrangement of each cassette and bioanalytical measurement conditions). A 5 h incubation ($n=5$ per cassette) was performed at 37°C in an incubated shaker (MaxQ4450 Thermo Fisher Scientific, NinoLab, Sweden) with a rotation speed of 45 rpm and constant oxygen flow of about 75–80 ml per minute through a glass frit. The viability of the brain slices was assessed using a dynamic pH measurement and lactate dehydrogenase activity release using a cytotoxicity detection kit (Roche Diagnostics GmbH, Germany).

Assuming that at equilibrium the concentration of the compounds in virtually protein free aECF is equal to the interstitial fluid concentration in the brain slice, the $V_{u,brain}$ (mL · g brain^{-1}) was estimated using Eq. 1 as a ratio of the amount of compound in the brain slice (A_{brain}, nmole · g brain^{-1}) to the measured final aECF

concentration (C_{buffer}, μmole · L^{-1}). The brain tissue density was assumed to be 1 g•ml^{-1}.

$$V_{u,brain} = \frac{A_{brain} - V_i \cdot C_{buffer}}{C_{buffer} \cdot (1 - V_i)} \quad (1)$$

where V_i (mL · g $brain^{-1}$) is the volume of the surrounding brain slices layer of aECF.

A volume of 0.094 mL ·g $brain^{-1}$ was obtained using [^{14}C] inulin as the marker by Fridén *et al.* (23).

A validation of $V_{u,brain}$ estimates from the brain slice method by use of the "gold" standard cerebral microdialysis was included in the study plan. However, due to a very low success rate of the microdialysis, it was not possible to complete the study. It is well-known that the sticking of compounds to microdialysis plastic tubing and probes is a major cause of failure. Accordingly, the adsorption of 30 compounds to the polyetheretherketone tubing was tested, dissolved in Ringer solution with and without 0.5% bovine serum albumin. Only eight compounds from the dataset went further to the subsequent evaluation of *in vitro* recovery from the CMA12 microdialysis probes. Finally, only four compounds were suitable for *in vivo* microdialysis. As this would not add enough information, the decision was made not to pursue this path further. This experience supports the opinion of a low throughput and utility of cerebral microdialysis in the drug discovery setting. Cerebral microdialysis of F3 and F4 (risperidone) was performed earlier in-house (unpublished data).

Equilibrium Dialysis

The fraction of unbound-compound in species-specific plasma ($f_{u,plasma}$) was determined using high-throughput ED according to van Liempd *et al.* (28). The fraction of unbound compound in rat brain homogenate $f_{u,brain}$ was assessed using a similar protocol with minor modifications (19,29). Briefly, compounds (5 μM) were added to brain homogenate diluted ten-fold (dilution factor, D), i.e. 1/9 w/v brain tissue with phosphate saline buffer (PBS). The brain homogenate was dialyzed against PBS pH 7.4 for 5 h using a Pierce Rapid Equilibrium Dialysis Device (RED) (Thermo Scientific, Rockford, IL, USA). Following incubation, samples were removed from both the buffer and brain homogenate sides to obtain free (unbound) and bound concentrations by LC-MS/MS analysis.

The unbound fraction of the compounds in the diluted (D) brain homogenate ($f_{u,hD}$) was calculated as:

$$f_{u,hD} = \frac{C_{buffer}}{C_{homogenate}} \quad (2)$$

where C_{buffer} represents the concentration measured in the buffer and $C_{homogenate}$ is the concentration measured in the brain homogenate.

The $f_{u,hD}$ is usually higher than the actual $f_{u,brain}$ as a result of the dilution. Therefore, $f_{u,hD}$ was corrected for the dilution factor (D, in this case 10 times) as described in Eq. 3 (30).

$$f_{u,brain} = \frac{f_{u,hD}}{D + f_{u,hD} - D \cdot f_{u,hD}} \quad (3)$$

P-gp Substrate Identification Assay

The *in vitro* passive permeability of test compounds and their ability to act as substrates for P-glycoprotein (P-gp) transport was evaluated using LLC-PK1 cells stably transfected with MDR1 in a trans-well system. The apical to basolateral (A to B) permeation rate (apparent permeability, P_{app}) of the test compounds (1 μM) was measured in the presence and absence of the P-gp inhibitor elacridar (5 μM) following an incubation period of 120 min (P_{app} ×10^{-6} cm·sec^{-1}). The integrity of the cellular monolayer was assessed in each incubation well through the inclusion of the fluorescent, low permeability marker compound, fluorescein.

In detail, LLC-MDR1 cells were seeded on 24-well cell culture inserts (Millicell®-PCF, 0.4 μm, 13 mm Ø, 0.7 cm^2) at ca 400 000 cells/cm^2. The cell culture medium consisted of Medium 199 supplemented with 10% fetal bovine serum and 100 U/ml penicillin/streptomycin. Five days after seeding, the test compounds were applied to the apical side of the monolayers to assess transport in the A to B direction in the presence and absence of elacridar. The medium used in the assay was Opti-MEM® (Gibco®, Life Technologies Corporation, Paisley, UK) with 1 w/v % bovine serum albumin. Inserts were incubated at 37°C in a humidified incubator containing 5% CO_2. Samples from the acceptor and donor compartments were collected after an incubation time of 120 min, to assess the permeability and to allow estimation of the test compound recovery during the experiment, respectively. The transport experiments were performed in triplicate. The test compound concentrations were measured using LC-MS/MS and quantified via a calibration curve.

The apparent permeability for each compound (P_{app}) in the absence and presence of elacridar was calculated from the following equation:

$$P_{app} = \frac{\left(dQ \middle/ dt\right)}{C0 \cdot A} \quad (4)$$

where dQ/dt is the rate of permeation of the drug across the monolayer, C_0 is the initial donor compartment concentration and A is the area of the cellular monolayer. If the ratio of the P_{app} (A to B) of the test compound in the presence of elacridar over P_{app} (A to B) of the test compound in the absence of elacridar was ≥2, then this suggests that P-gp mediated efflux.

In Vivo NeuroPK Studies

Taking into consideration the time-dependency of the brain partitioning, $K_{p,brain}$ should preferably be determined using steady-state total brain and plasma concentrations after constant-rate intravenous infusion. Alternatively, $K_{p,brain}$ can be assessed as the ratio of the areas under the total drug brain to plasma concentration-time curves ($AUC_{tot,brain}$/$AUC_{tot,plasma}$), using various time points after administration of a single dose. With the intention to specify the conditions under which the brain exposure has been measured in the present study, $K_{p,brain,SD}$ is used to denote single dose administration (SD) and $K_{p,brain,SS}$ is used to denote an intravenous constant-rate infusion (steady-state, SS).

Single Dose Studies. The *in vivo* brain distribution experiments were part of larger plasma pharmacokinetic and tissue distribution studies. $K_{p,brainSD}$ was determined at multiple time points (minimum four) after oral (PO) or subcutaneous (SC) administration. The dose ranges selected for these studies were linked with the doses used in the corresponding PD studies and, consequently, varied among the different study protocols from 5 to 30 mg/kg (Supplementary Material, Table SII). Generally, samples were taken at 30 min, 1, 2, 4, 7 and 24 h after dose administration. The preference of using Sprague Dawley rats or Swiss mice for the neuroPK study was based on relevant and accessible pharmacodynamic models in these animals. At the designated time points, the rats/mice ($n=3$) were anaesthetized and blood samples were immediately collected into 10-ml BD K3EDTA vacutainers (BD Biosciences, Plymouth, UK). Subsequently, animals were sacrificed, the brain was rapidly removed, and homogenized in demineralized water (1/9 w/v). Plasma and brain homogenate samples were stored at −20°C pending analysis using LC-MS/MS. The $K_{p,brainSD}$ was calculated from the areas under the curve (AUC_{0-t}) for total drug brain and plasma concentrations.

Constant-Rate Intravenous Infusion Studies. To test the validity of the use of the brain partitioning coefficient $K_{p,brainSD}$, a constant-rate intravenous infusion study was conducted. Seven compounds (A1, B1, B4, D1, D4, G2, and G5) covering a wide range of $K_{p,uu,brain}$ values were selected (Supplementary Material, Table II and SIII). The drugs were administered in cassettes consisting of two compounds in 20% 2-hydroxypropyl-β-cyclodextrin as over-night constant-rate intravenous infusions, using a flow rate of 1 $mL/kg{\cdot}h^{-1}$ (Supplementary Material, Table SIII).

Three male Sprague Dawley rats catheterized in the femoral vein were used per cassette. Blood sampling from the tail vein at 1 h, 2 h and at the end of the infusion (19.5 to 20.5 h after the start of infusion, Table SIII) was used to confirm attainment of steady-state conditions. At the end of the experiment, the rats were anaesthetized and CSF was collected from the *cisterna magna*. Blood samples were immediately collected into 10-ml BD K3EDTA vacutainers (BD Biosciences, Plymouth, UK) using intracardial puncture. After that, the rats were sacrificed through exsanguination by fast severing of the abdominal aorta. The blood samples were placed on ice, and plasma was obtained following the centrifugation at 4°C for 10 min at 1900 g. The brain was rapidly removed, rinsed with PBS and dissected. Brain tissue samples were homogenized in demineralized water (1/9 w/v) and stored at −20°C prior to analysis. $K_{p,uu,brainSS}$ was estimated using total drug brain and plasma concentrations corrected for nonspecific binding. $K_{p,uu,CSF}$ was assessed using CSF and plasma drug concentrations corrected for nonspecific binding (31).

Bioanalytical Procedures

The bioanalysis of samples from the brain slice assay was performed using reversed-phase liquid chromatography followed by detection with a tandem mass spectrometer (LC-MS/MS) Quattro Ultima, (Micromass, Manchester, UK). The LC system consisted of an LC-10AD pump (Shimadzu, Kyoto, Japan) and a SIL-HTc autosampler (Shimadzu, Kyoto, Japan). LC-MS/MS measurement conditions for all sample processing and compound-specific bioanalytical parameters are summarized within Supplementary Material, Table SI. Sample processing was performed using the MassLynx software, version 4.0 (Micromass, Manchester, UK). Acetonitrile, formic acid, ammonium formate and ammonium acetate were purchased from Merck (Darmstadt, Germany). The water was purified using a Milli-Q system (Millipore, Bedford, Massachusetts). Individual standard curves were prepared in respective control matrices. An appropriate dynamic range was achieved for all assays, and instrument settings and potentials were adjusted to optimize the mass spectrometer signal for each analyte.

Quantitative bioanalysis of samples from the supporting assays; equilibrium dialysis ($f_{u,plasma}$ and $f_{u,brain}$), the P-gp substrate identification assay and the *in vivo* neuroPK studies was also performed using reversed-phase HPLC followed by detection (LC-MS/MS) using comparable approaches and similar equipment to that described for the brain slice sample analysis (specific details not included).

Data Analysis

Normally distributed values (Kolmogorov-Smirnov test) are presented as a mean and standard deviation (SD). Non-normally distributed values are presented as a median and

Table II Unbound Fraction of Drug in Brain Homogenate ($f_{u,brain}$) and Species-Specific Plasma ($f_{u,plasma}$), Volume of Distribution of Unbound-Drug in Brain ($V_{u,brain}$; mL·g brain^{-1}), $V_{u,brain}$ Predicted from the Fraction of Unbound-Drug in Brain Homogenate Utilizing pH Partitioning Model ($1/f_{u,brain,corrected}$) as well as Ratios of Observed Brain Intra- to Extracellular Unbound-Drug Concentrations ($K_{p,uu,cell,obs}$), Brain Interstitial Fluid to Plasma Unbound-Drug Concentrations ($K_{p,uu,brain}$) and Total Brain to Total Plasma Drug Concentrations ($K_{p,brain}$) of the set of 40 Compounds

ID	$f_{u,brain}$	$f_{u,plasma}$	$V_{u,brain}$	$1/f_{u,brain,corrected}$	$K_{p,uu,cell,obs}$	$K_{p,uu,brain}$	$K_{p,brain}$
A1	0.15	0.261	4.88 ± 0.49	6.68	0.73 ± 0.073	0.46	0.58
A2	0.17	0.207	5.54 ± 0.37	5.88	0.94 ± 0.063	0.96	1.1
A3	0.30	0.395	2.77 ± 0.31	3.33	0.83 ± 0.094	0.50	0.55
B1	0.0005	0.0035	624 ± 85.5	2001	0.31 ± 0.043	2.01	4.4
B2	0.14	0.310	6.69 ± 0.92	7.40	0.94 ± 0.129	0.53	1.1
B3	0.10	0.305	6.0 ± 0.55	10.0	0.60 ± 0.055	0.18	0.33
B4	0.30	0.520	3.29 ± 0.42	3.33	0.99 ± 0.127	0.13	0.23
B5	0.02	0.056	36.1 ± 2.96	146	0.72 ± 0.059	0.02	0.04
C1	0.0049	0.015	140 ± 9.76	213	0.69 ± 0.048	0.29	0.6
C2	0.02	0.052	42.1 ± 2.62	54.5	0.84 ± 0.052	0.09	0.2
C3	0.02	0.062[b]	34.5 ± 3.34	51.9	0.69 ± 0.067	0.37	0.8
D1	0.0038	0.006	189 ± 24.5	263	0.72 ± 0.093	0.79	0.9
D2	0.012	0.056	57.5 ± 5.55	83.4	0.70 ± 0.067	0.71	2.3
D3	0.005	0.013	216 ± 19.9	249	1.02 ± 0.094	0.85	2.4
D4	0.0009	0.0021	362 ± 35.4	1111	0.33 ± 0.032	1.58	1.2
E1	0.055	0.086	13.3 ± 0.97	18.2	0.73 ± 0.053	0.61	0.7
E2	0.04	0.083	20.9 ± 1.77	25.0	0.84 ± 0.071	0.86	1.5
F1	0.033	0.139	22.0 ± 3.15	30.3	0.73 ± 0.104	0.28	0.85
F2	0.03	0.226	34.6 ± 4.25	80.2	1.04 ± 0.128	1.53	12
F3	<0.0005[a]	0.239	80.1 ± 6.83		0.04 ± 0.003[a]	0.94	18
F4	0.10	0.118	13.5 ± 2.65	26.7	1.37 ± 0.269	0.19	0.3
F5	0.119	0.285	10 ± 0.58	22.6	1.19 ± 0.069	0.039	0.11
F6	0.089	0.113	50.5 ± 9.06	61.0	4.48 ± 0.803	0.84	4.8
G1	0.044	0.280[b]	52.8 ± 8.59	55.9	2.32 ± 0.378	0.044	0.65
G2	0.02	0.155[b]	96.5 ± 17.9	125	1.93 ± 0.359	0.19	2.8
G3	0.009	0.038	191 ± 18.8	243	1.72 ± 0.169	0.083	0.6
G4	0.15	0.410[b]	12.8 ± 1.67	17.9	1.93 ± 0.251	0.019	0.1
G5	0.023	0.230[b]	113 ± 21.9	125	2.60 ± 0.504	0.044	1.14
G6	0.24	0.520[b]	14.8 ± 2.06	11.6	3.56 ± 0.495	0.83	6.4
G7	0.03	0.264	81.8 ± 4.39	81.8	2.45 ± 0.132	0.034	0.73
G8	0.149	0.322	39.4 ± 5.17	16.9	5.87 ± 0.771	0.024	0.3
G9	0.256	0.419[b]	17.1 ± 3.04	9.19	4.38 ± 0.778	0.028	0.2
G10	0.099	0.361[b]	12.9 ± 0.96	21.1	1.28 ± 0.095	0.03	0.14
H1	0.287	0.776	29.1 ± 4.09	31.5	8.36 ± 1.17	0.049	1.1
H2	0.21	*N.A.*	115 ± 16.9	88.7	24.1 ± 3.56	*N.A.*	11
I1	0.10	0.450	2.91 ± 0.19	10.0	0.29 ± 0.019	0.23	0.3
I2	0.0005	0.005	308 ± 59.4	2000	0.15 ± 0.030	0.97	1.5
I3	0.10	0.087	10.9 ± 0.74	10.0	1.09 ± 0.074	0.32	0.3
I4	0.11	0.069	6.32 ± 0.79	9.09	0.70 ± 0.087	0.92	0.4
I5	0.043	0.073	14 ± 2.16	23.3	0.60 ± 0.093	0.49	0.5

[a] $f_{u,brain}$ of F3 below the accuracy level of brain tissue binding assay (0.0005)

[b] $f_{u,plasma}$ was measured using mouse plasma

N.A. not available

interquartile range (IQR). For the comparison of median values, a Kruskal Wallis test followed by a Dunn's multiple comparison test was used. Wilcoxon matched-pairs signed rank test was used to compare $f_{u,brain}$ and $f_{u,brain,corrected}$.

NeuroPK Parameters

Unbound-Drug Brain Partitioning Coefficient, $K_{p,uu,brain}$

The assessment of the steady-state ratio of brain ISF to plasma unbound-drug concentrations $K_{p,uu,brain}$ was achieved by correction of the total brain to total plasma drug concentrations ratio $K_{p,brain}$ for nonspecific brain tissue and plasma protein binding (9,14,22). This approach is defined as a combinatory mapping of $K_{p,uu,brain}$. The combination of the three compound-specific parameters $K_{p,brain}$ measured in rodents *in vivo*, $V_{u,brain}$ obtained using the fresh rat brain slice method and $f_{u,plasma}$ determined in species-specific plasma using ED, was used for calculation of $K_{p,uu,brain}$ for the set of 40 compounds.

$$K_{p,uu,brain} = \frac{K_{p,brain}}{V_{u,brain} \cdot f_{u,plasma}} \quad (5)$$

$K_{p,uu,brain}$ values closer to unity describe a mainly passive transport at the BBB or reflect similar efflux and influx clearances (9,14). $K_{p,uu,brain}$ values smaller than unity indicate predominantly active efflux, and $K_{p,uu,brain}$ values exceeding unity indicate potential active uptake.

The $K_{p,uu,brain}$ values characterizing BBB net flux were used in evaluating possible clinical success from a perspective of $C_{u,brainISF}$ linked to pharmacological potency (e.g. the inhibitory constant in nM) and an intra-brain target engagement measure (e.g. receptor occupancy) of the compound in relation to potential attainable concentrations of unbound-drug in plasma ($C_{u,plasma}$) as described by:

$$C_{u,brainISF} = K_{p,uu,brain} \cdot C_{u,plasma} \quad (6)$$

$C_{u,brainISF}$ was further used for evaluation of receptor occupancy (%) as:

$$\text{Receptor occupancy} = \frac{C_{u,brainISF}}{C_{u,brainISF} + K_d} \cdot 100 \quad (7)$$

where the constant of dissociation K_d (alternatively the inhibitory constant K_i) is an *in vitro* estimate of the pharmacological potency.

Unbound-Drug Cell Partitioning Coefficient, $K_{p,uu,cell}$

Direct estimation of the steady-state unbound-drug intracellular-to-extracellular partitioning coefficient ($K_{p,uu,cell}$) is currently unrealistic due to the technical issues associated with the measurement of intracellular unbound-drug concentrations. Instead, approximation of $K_{p,uu,cell}$ was accomplished by combining $V_{u,brain}$ and $f_{u,brain}$ information using Eq. 8 and referred to as the observed $K_{p,uu,cell,obs}$ (13).

$$K_{p,uu,cell,obs} = V_{u,brain} \cdot f_{u,brain} \quad (8)$$

In general, $K_{p,uu,cell,obs}$ describes the steady state relationship of unbound-drug intracellular-to-extracellular concentrations and indicates the average concentration ratio for all cell types within the brain. The $K_{p,uu,cell,obs}$ assessment concept is based on the divergences in the nature of the measurements obtained from the brain slice and brain homogenate methods. The major determining factor of $f_{u,brain}$ comprises nonspecific binding of compound to various intracellular lipids and proteins (assuming that the expression level of specific targets is negligible). $V_{u,brain}$ provides information on overall uptake of the compound by brain parenchymal cells, i.e. nonspecific and specific binding, active transport, pH partitioning etc.

Unbound-Drug Cell Partitioning and Beyond: $K_{p,uu,cell,pred}$, $K_{p,uu,cyto,pred}$ and $K_{p,uu,lyso,pred}$

Based on the statement that only non-ionized unbound drug molecules are able to pass the cellular membranes, the unbound-drug cell partitioning coefficient could also be predicted using the pH partition theory (13). The ionization stage of the compounds is pH-dependent and driven by a physiological pH gradient between plasma (pH7.4), ISF (pH7.3), cytoplasm (pH ~ 7) and acidic subcellular compartments such as e.g. lysosomes (pH ~ 5).

A three-compartment pH partitioning model of $K_{p,uu,cell,pred}$, where "pred" stands for predicted values, was used for the prediction of the unbound drug cell partitioning coefficient (25). The model is based on the pKa of the compounds, physiological volumes as well as on the pH of the relevant compartments: plasma, cytoplasm and lysosomes,

$$K_{p,uu,cell,pred} = V_{ISF} + K_{p,uu,cyto,pred} \cdot \left(V_{cyto} + V_{lyso} \cdot K_{p,uu,lyso,pred}\right) \quad (9)$$

where V_{ISF}, V_{cyto}, and V_{lyso} are the physiological volumes of the ISF (0.20 mL·g brain^{-1}), cytosol (0.79 mL·g brain^{-1}), and lysosomes (0.01 mL·brain^{-1}), respectively (32). The ratios of cytosolic to extracellular unbound-drug concentrations ($K_{p,uu,cyto,pred}$) and lysosomic to cytosolic unbound-drug concentrations ($K_{p,uu,lyso,pred}$) for the bases were calculated as:

$$K_{p,uu,cyto,pred} = \frac{10^{pKa-pH_{cyto}} + 1}{10^{pKa-pH_{ISF}} + 1} \quad (10)$$

$$K_{p,uu,lyso,pred} = \frac{10^{pKa-pH_{lyso}} + 1}{10^{pKa-pH_{cyto}} + 1} \quad (11)$$

where pH_{cyto}=7.06, pH_{ISF}=7.3 and pH_{lyso}=5.18, as determined by Fridén and co-workers (25).

Using Eq. 8, $K_{p,uu,cell,pred}$ predicted from the three-compartment model was applied to more accurately approximate intra-brain distribution and binding from $f_{u,brain}$ measurements. To make a clear distinction between the experimentally determined $V_{u,brain}$ values and those predicted from $f_{u,brain}$ values corrected for lysosomal trapping, the latter is termed $1/f_{u,brain,corrected}$.

$$\frac{1}{f_{u,brain,corrected}} = \frac{K_{p,uu,cell,pred}}{f_{u,brain}} \quad (12)$$

Based on the inverse relationship between $f_{u,brain}$ and $V_{u,brain}$, the $1/f_{u,brain,corrected}$ values were used for comparison of the performance of the brain homogenate and brain slice methods for the 40 compounds. The $1/f_{u,brain,corrected}$ values have been proposed for use in the calculation of $K_{p,uu,brain}$ when $V_{u,brain}$ measurements are lacking, as derived from Eq. 5 (25):

$$K_{p,uu,brain} \approx \frac{K_{p,brain}}{\frac{1}{f_{u,brain,corrected}} \cdot f_{u,plasma}} \quad (13)$$

RESULTS

Assessment of CNS Exposure, $K_{p,uu,brain}$

The extent of BBB transport of the 40 compounds as estimated by $K_{p,uu,brain}$ varied from 0.02 to 2.0, a 100-fold range (Fig. 1 and Table II). Most compounds exhibited efflux at the BBB with 60% of the drug candidates having $K_{p,uu,brain}$ below 0.5. Only 10 of these 24 compounds were identified as P-gp substrates *in vitro*. Three out of the 40 compounds (B1, D4, F2) had $K_{p,uu,brain}$ values exceeding unity, indicating active uptake. $K_{p,uu,brain}$ varied extensively also within some groups of compounds designed for the same pharmacological target, e.g. Groups B, C, F and G (Fig. 1).

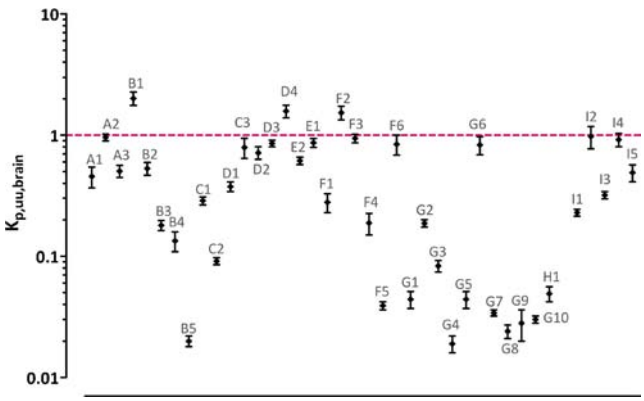

Fig. 1 Ratio of brain interstitial fluid to plasma unbound-drug concentrations $K_{p,uu,brain}$ for the set of 40 compounds. $K_{p,uu,brain}$ equal to unity is indicated as a red dashed line. Compounds exhibiting $K_{p,uu,brain}$ lower than unity are subject to predominant active efflux.

Evaluation of the ratios of total brain to total plasma drug concentrations for the dataset revealed a 450-fold range in $K_{p,brain}$ values, compared to the 100-fold range in $K_{p,uu,brain}$ values (Fig. 2 and Table II). The linear regression analysis showed no direct relationship between $K_{p,brain}$ and $K_{p,uu,brain}$ ($R^2 = 0.25$) as displayed in Fig. 2. This is to be expected as $K_{p,brain}$ is also determined by $f_{u,plasma}$ and $V_{u,brain}$ (Eq. 5). Some compounds with $K_{p,brain}$ values below unity actually have $K_{p,uu,brain}$ values that are quite high, and compounds with $K_{p,brain}$ around or above unity have very low $K_{p,uu,brain}$ values.

The assessment of $K_{p,uu,brain}$ using the rapid mapping approach (Eq. 5) is strongly dependent on the *in vivo* measurement of the brain partitioning coefficient $K_{p,brain}$ often determined after a single dose ($K_{p,brainSD}$) when an equilibration across the BBB may or may not have been reached. Seven of the compounds (A1, B1, B4, D1, D4, G2, and G5) were therefore selected for confirmatory constant-rate intravenous infusion experiments. These compounds covered a wide range of $K_{p,uu,brain}$ from 0.044 to 2.0 (Table II). The comparison of $K_{p,brainSD}$ with $K_{p,brainSS}$ attained after a constant-rate intravenous infusion revealed good agreement between the two methods, not exceeding the 2-fold prediction error threshold (Supplementary Material, Figure S1 and Table SIII). Overall, the results point out that $K_{p,brainSD}$ is a good enough measurement of steady-state brain partitioning coefficient and therefore the $K_{p,brainSD}$ was used in the present study.

Evaluation of Intra-Brain Distribution

The $V_{u,brain}$ varied from 2.8 to 624 mL· g brain^{-1} for the studied dataset, revealing extensive inter-compound variability in binding to brain tissue components (Table II and Fig. 3). All compounds had $V_{u,brain}$ values above 1 mL· g brain^{-1} demonstrating extensive intracerebral distribution. Thirty-one of the forty compounds revealed $V_{u,brain}$ values higher than 10 mL· g brain^{-1}. Interestingly, a similar magnitude of inter-compound variability was observed among some of the chemical analogues within a group as compared to between the groups, for instance within the P2X7 antagonists, Group I, where $V_{u,brain}$ varied between 2.9 and 308 mL· g brain^{-1}.

The $f_{u,brain}$ varied 600-fold from 0.0005 to 0.3 (Table II). Thirty-two of the compounds exhibited $f_{u,brain}$ values lower than 0.1. The estimated $f_{u,brain}$ of F3 was below the accuracy level of the brain homogenate assay (lower than 0.0005). It was therefore removed from all related analyses. Interestingly, the $V_{u,brain}$ of F3 was 80 mL· g brain^{-1} corresponding to an $f_{u,brain,corrected}$ of 0.0125, which deviated significantly from the extremely low $f_{u,brain}$ measurement. Moreover, in spite of the fact that the $f_{u,brain}$ and $f_{u,brain,corrected}$ are significantly correlated ($r^2 = 0.858$, $p < 0.0001$) the median values are

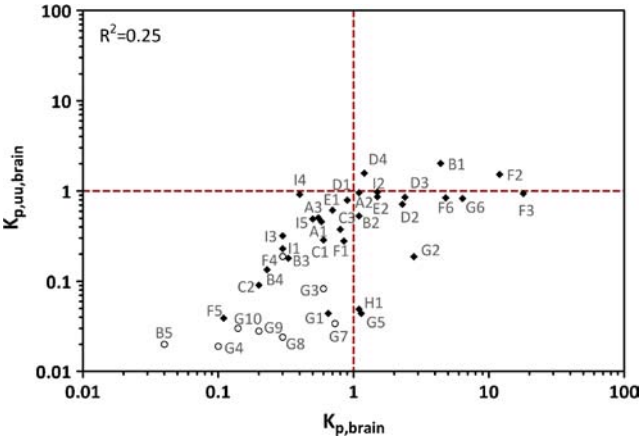

Fig. 2 The relationship between the ratio of total brain to total plasma drug concentrations ($K_{p,brain}$) and the ratio of brain interstitial fluid to plasma unbound-drug concentrations ($K_{p,uu,brain}$). $K_{p,brain}$ and $K_{p,uu,brain}$ equal to unity are indicated as a red dashed lines. R^2 is a coefficient of determination of the linear regression analysis. Empty circles represent the P-gp substrates identified in an *in-vitro* P-gp substrate assay (occurrence of P-gp mediated efflux is based on the ratio $\frac{Papp\ A-B\ (+Pgp\ inhibitor)}{Papp\ A-B\ (-Pgp\ inhibitor)} \geq 2$).

significantly different (Wilcoxon matched-pairs signed rank test $p<0.0001$), i.e. $f_{u,brain}$ (median 0.0495, IQR 0.0199–0.147) *vs* $f_{u,brain,corrected}$ (median 0.0324, IQR 0.008–0.097).

A comparison was made between the intracerebral distribution parameters estimated using the brain slice and the brain homogenate methods; the correction for pH partitioning was applied to compensate the brain homogenate results for the lysosomal trapping phenomenon (Fig. 4). A strong linear relationship ($R^2=0.79$; $p<0.0001$) between $V_{u,brain}$ and $1/f_{u,brain,corrected}$ was found. However, a trend towards an over-prediction of $V_{u,brain}$ by using $1/f_{u,brain,corrected}$ was apparent.

Estimation of Intracellular Distribution

Calculating $K_{p,uu,cell,obs}$ from the combination of brain slice and brain homogenate measurements using Eq. 8 revealed a

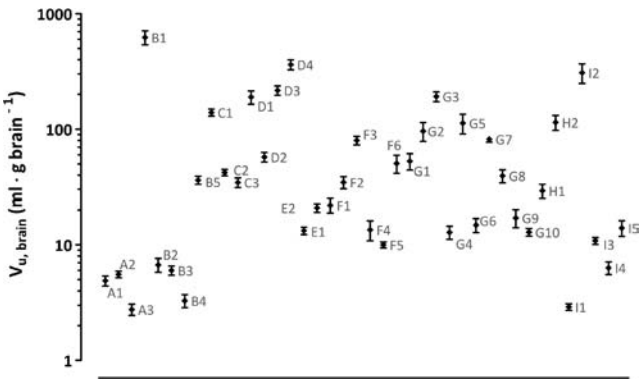

Fig. 3 Volume of distribution of unbound drug in brain (mL g brain^{-1}) for the set of 40 compounds estimated using the brain slice method. Data presented as a mean and standard deviation based on $n=25$ per compound.

widespread difference (160-fold) in intracellular distribution of the studied compounds, with values of 0.15 to 24 (Fig. 5 and Table III).

The unbound-drug cell partitioning coefficient for bases was significantly higher ($p<0.0001$) compared with neutral compounds with a median $K_{p,uu,cell,obs}$ of 2.1 (IQR 1.2–4.4). Compounds with primary intracellular pharmacological targets showed a trend towards higher $K_{p,uu,cell,obs}$ values, i.e. the median $K_{p,uu,cell,obs}$ for compounds targeting extracellular G-protein coupled receptors was 0.72 (IQR 0.6–1.2) as opposed to 0.98 (IQR 0.7–2.4) for the compounds designed for intracellular targets. Comparing the observed $K_{p,uu,cell,obs}$ values (Eq. 8) with the predicted ones (Eq. 9) some deviations were observed (Table III). Overall, the predicted $K_{p,uu,cell,pred}$ values from the three-compartment partitioning model (Eq. 9) were smaller and varied only 18-fold, from 1.0 to 18 (Table III), compared with the 160-fold difference for $K_{p,uu,cell,obs}$ presented above.

Dividing intracellular distribution further into the components of cytosolic and lysosomal partitioning was performed using the pH partitioning theory (Eqs. 10 and 11). The range of $K_{p,uu,cyto,pred}$ values was from 1.0 to 1.73 (Table III). This can be explained by the small pH differences between ISF (pH ~ 7.3) and ICF (pH ~ 7.0). On the contrary, $K_{p,uu,lyso,pred}$ varied 75-fold with 18 of the 40 compounds showing lysosomic to cytosolic unbound-drug concentrations ratios higher than 50.

Interplay of NeuroPK Parameters

The main neuroPK parameters are $K_{p,uu,brain}$, $K_{p,uu,cell}$ and $K_{p,uu,CSF}$ supported by information on $V_{u,brain}$ (or $1/f_{u,brain,corrected}$) and $f_{u,plasma}$. To further understand the relationship between some of these parameters, several comparisons were made.

A linear regression analysis between $K_{p,uu,brain}$ and $K_{p,uu,cell,obs}$ showed no relationship (Fig. 6), indicating that the BBB transport as described with $K_{p,uu,brain}$ and the equilibration across the cellular barriers as characterized by $K_{p,uu,cell,obs}$ are two independent properties of the compounds studied.

The properties governing brain tissue binding and uptake *vs.* BBB transport are illustrated in Fig. 7. It is clear from the figure that these two parameters are independent of each other indicating that they are determined by different characteristics. It is therefore not possible to use $V_{u,brain}$ (or $1/f_{u,brain,corrected}$) to predict BBB transport. The BBB transport needs to be measured separately.

$f_{u,plasma}$ has also been proposed as a predictor for brain penetration (33). Figure 8 shows that this is not the case and again, if BBB transport is of interest, it needs to be specifically measured.

Assessing CSF for the prediction of BBB transport was evaluated for seven compounds (Supplementary Material,

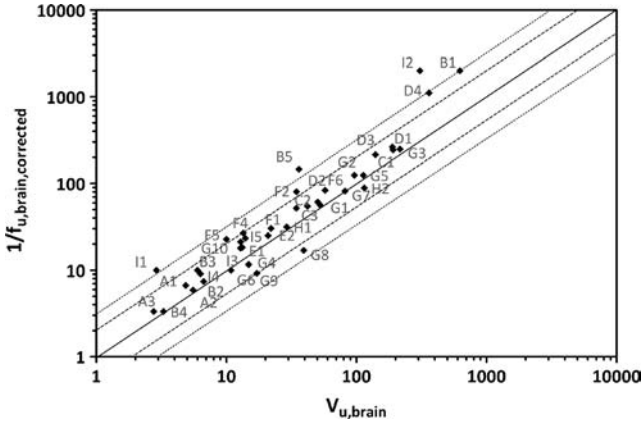

Fig. 4 The volume of distribution of unbound compound in brain ($V_{u,brain}$) measured using the brain slice method plotted versus the inverse fraction of unbound compound based on brain homogenate binding, corrected for pH partitioning ($1/f_{u,brain,corrected}$). F3 was removed from the analysis as the obtained value of $f_{u,brain}$ was below the accuracy level of brain tissue binding assay (0.0005). The solid line describes the line of identity and the dashed lines correspond to two and three-fold deviations from line of identity, respectively.

Table SIII). The data showed a strong relationship between $K_{p,uu,CSF}$ and $K_{p,uu,brain}$ with a coefficient of determination $R^2 = 0.88$ (Supplementary Material, Figure S2). However, the $K_{p,uu,CSF}$ of the two strong P-gp substrates B4 and G2 was over-predicting $K_{p,uu,brain}$ by 2.6- and 3.3-fold, respectively.

The mapping of processes governing the drug concentrations in the brain requires input from multiple modalities, each providing a unique piece of evidence essential to unfold the drug disposition pattern of individual compounds (Fig. 9). It was possible to use this approach for the fast and relatively easy determination of the main neuroPK parameters.

A visualization of the steady-state unbound concentrations in the different brain compartments can be considered as an additional advantageous tool for drug discovery (Fig. 10). Linking the obtained target-site concentrations to *in vitro* PD

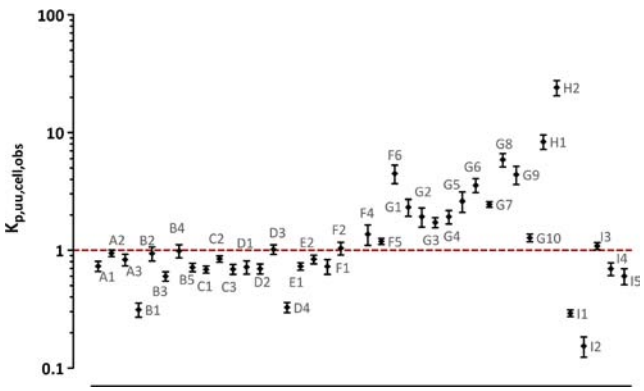

Fig. 5 The ratio of brain intra- to extracellular unbound-drug concentrations $K_{p,uu,cell,obs}$ for the set of 40 compounds. $K_{p,uu,cell}$ equal to unity is indicated as a red dashed line. $K_{p,uu,cell}$ higher than unity reflects intracellular accumulation. This accumulation can be caused by trapping of compounds in acidic subcellular compartments (e.g. lysosomes) or by active uptake into the cells.

measurements can facilitate the decision-making and calculation of the dose requirements for CNS action or prevention of CNS side effects. Figure 10 illustrates these relationships for the PDE10 inhibitor A1.

DISCUSSION

An in-depth integrative neuroPK analysis was made for a novel dataset of 40 compounds with the aim to contribute to the clinically important mechanistic understanding of brain drug disposition in drug discovery. This was accomplished through evaluation of the compounds' BBB net flux ($K_{p,uu,brain}$), intra-brain distribution and brain tissue binding ($V_{u,brain}$) as well as intra- and sub-cellular partitioning (observed and predicted $K_{p,uu,cell}$, $K_{p,uu,cyto,pred}$, $K_{p,uu,lyso,pred}$). Also, our study was inspired by the desire to work within a short time-frame, which is necessary for the preclinical screening of NCEs, without compromising the quality of the analysis.

The overwhelming importance of neuroPK studies is to project the brain target-site concentration of the compound in relation to the systemic drug exposure and pharmacodynamic readouts in the early stages of drug discovery and development. Hence, the assessment of $K_{p,uu,brain}$ is a critical step in the evaluation of NCE BBB transport (9). In the present study, a clinically relevant picture of $K_{p,uu,brain}$ for each of the compounds was obtained through the multidimensional evaluation of the PK parameters $K_{p,brain}$, $V_{u,brain}$, and $f_{u,plasma}$; i.e. via the combinatory mapping approach suitable for an industrial setting. The estimates of $K_{p,uu,brain}$ were subsequently used for ranking, based on the BBB penetration properties of the NCEs. The obtained individual $K_{p,uu,brain}$ values varied100-fold with a prevalence of compounds having active efflux at the BBB. Nevertheless, for the absolute go/no-go decision, it is crucial to bear in mind, that the use of any strict cut-off for $K_{p,uu,brain}$ is pointless and flawed. For instance, the atypical antipsychotic risperidone (F4) exhibited a low BBB penetration ability with a $K_{p,uu,brain}$ of 0.19 (Table II), meaning that less than 20% of the unbound-drug in plasma is entering into the brain. The $C_{u,brainISF}$ of risperidone estimated from $C_{u,plasma}$ using Eq. 6 was 1.51 nM at the maximal plasma concentration after administration of 10 mg/kg to rats. Despite being a P-gp substrate, the achieved $C_{u,brainISF}$ of risperidone was pharmacologically significant i.e. it reached the receptor binding affinity measured *in vitro*. Correspondingly, the affinity assessed by direct *in vitro* measurement of D_2 receptor dissociation rate in the presence of 10 μM raclopride was 1.13 nM (unpublished observation). Moreover, using Eq. 7 the occupancy of D_2 receptors was estimated to be about 57%, which is proven to be sufficient for initiation of a therapeutic response (18). As an alternative example, the positive allosteric modulator of $mGlu_2$ (D4) with

Table III Ion Class, Predicted by Three-Compartment pH Partitioning Model Ratio of Cytosolic to Extracellular Unbound-Drug Concentrations ($K_{p,uu,cyto,pred}$), Ratio of Lysosomic to Cytosolic Unbound-Drug Concentrations ($K_{p,uu,lyso,pred}$), Ratio of Brain ICF to ISF Unbound-Drug Concentrations ($K_{p,uu,cell}$) and Experimentally Determined Observed $K_{p,uu,cell}$ of 40 Structurally Diverse Compounds

ID	Ion Class	$K_{p,uu,cyto,pred}$	$K_{p,uu,lyso,pred}$	$K_{p,uu,cell}$	
				Predicted	Observed
A1	weak base	1.00	1.16	1.00	0.73
A2	weak base	1.00	1.00	1.00	0.94
A3	weak base	1.00	1.05	1.00	0.83
B1	weak base	1.00	1.07	1.00	0.31
B2	weak base	1.01	3.51	1.04	0.94
B3	neutral	1.00	1.00	1.00	0.60
B4	weak base	1.00	1.00	1.00	0.99
B5	weak base	1.73	75.52	2.90	0.72
C1	weak base	1.02	4.27	1.05	0.69
C2	base	1.04	7.00	1.09	0.84
C3	weak base	1.01	3.51	1.04	0.69
D1	neutral	1.00	1.00	1.00	0.72
D2	weak base	1.00	1.65	1.01	0.70
D3	base	1.07	11.87	1.17	1.02
D4	neutral	1.00	1.00	1.00	0.33
E1	neutral	1.00	1.00	1.00	0.73
E2	neutral	1.00	1.00	1.00	0.84
F1	weak base	1.00	1.02	1.00	0.73
F2	base	1.55	63.41	2.41	1.04
F3	base	1.66	71.12	2.69	0.04[a]
F4	base	1.66	71.22	2.71	1.37
F5	base	1.66	70.80	2.68	1.19
F6	base	1.62	68.15	5.41	4.48
G1	base	1.57	64.99	2.46	2.32
G2	base	1.58	65.82	2.49	1.93
G3	base	1.46	56.91	2.19	1.72
G4	base	1.66	70.80	2.68	1.93
G5	base	1.73	75.33	2.87	2.60
G6	base	1.69	73.24	2.78	3.56
G7	base	1.57	64.77	2.45	2.45
G8	base	1.59	66.40	2.51	5.87
G9	base	1.53	61.91	2.35	4.38
G10	base	1.42	53.47	2.09	1.28
H1	base	1.70	73.29	9.04	8.36
H2	base	1.71	74.14	18.62	24.12
I1	neutral	1.00	1.00	1.00	0.29
I2	neutral	1.00	1.00	1.00	0.15
I3	neutral	1.00	1.00	1.00	1.09
I4	neutral	1.00	1.00	1.00	0.70
I5	neutral	1.00	1.00	1.00	0.60

[a] $f_{u,brain}$ of F33 below the accuracy level of brain tissue binding assay (0.0005)

a $K_{p,uu,brain}$ of 1.58 (probable active uptake) could be discussed (Table II). The maximal $C_{u,plasma}$ after oral administration of 10 mg/kg in rats was about 30 ng/mL. Consequently, the projected $C_{u,brainISF}$ was 46 ng/mL (about 120 nM) which was also above the EC_{50} value of 81 nM obtained in an *in vitro* functional assay (unpublished observation). Therefore, practically it is essential to utilize $K_{p,uu,brain}$ in relation to the pharmacodynamic readouts. However, when relating unbound-drug ISF concentrations to *in vitro* PD measurements, one has to keep in mind to correct for the potential nonspecific binding in the *in vitro* assay, particularly for compounds with a high nonspecific binding to proteins.

In light of the earlier observed trend to use $K_{p,brain}$ as the main parameter for the evaluation of brain penetration ability of NCEs, it is important to mention that this strategy is potentially erroneous and, hence, not to be recommended. This is due to the fact that $K_{p,brain}$ is determined by the three independent properties of the drug: BBB transport, intrabrain distribution and plasma protein binding. Primarily, high $K_{p,brain}$ values may be intimately linked to a profound nonspecific binding of the compound to proteins in brain and blood tissues, but not to an extensive BBB transport or vice versa. For instance, compounds D4 and H1 are analogous by means of their $K_{p,brain}$ values (1.2 and 1.1, respectively). However, there is a dramatic divergence in their BBB net flux, i.e. their $K_{p,uu,brain}$ values are1.58 and 0.049, respectively. Hence, it is much more likely that D4 would have a higher potential as CNS drug, given similar target potency. Comparison of G8 and I4 could be another illustration of a potential flaw associated with estimation of BBB transport based on $K_{p,brain}$ values (Table II and Fig. 2). Specifically, G8 had a $K_{p,brain}$ value of 0.3 but a $K_{p,uu,brain}$ of only 0.024, compared to I4 with a $K_{p,brain}$ of 0.4 and a $K_{p,uu,brain}$ of 0.92. In summary, the lack of any relationship between $K_{p,brain}$ and $K_{p,uu,brain}$ (Fig. 2) supports the use of the more BBB transport focused parameter $K_{p,uu,brain}$ for decision making when selecting optimal compounds regarding CNS penetration. For non-CNS targets it may be as important to select compounds with low $K_{p,uu,brain}$ to avoid potential CNS side effects, as for CNS targets to select compounds with higher $K_{p,uu,brain}$, to avoid peripheral side effects.

The presence of efflux transporters at the BBB such as the ATP-binding cassette transporters superfamily, e.g. P-gp, breast cancer resistance-associated protein (BCRP) and multidrug resistance-associated proteins makes targeting of the brain very demanding. In pharmaceutical industry, this issue is often addressed by studying various cell monolayers stably expressing human P-gp (rarely BCRP), followed, if necessary, by examination of brain PK behavior of the NCEs in rodent transgenic and/or chemical knock out models. However, the ultimate translational value of these types of investigations is contradictory and often controversial. In the studied dataset, 24 out of the 40 compounds exhibited active efflux at the BBB

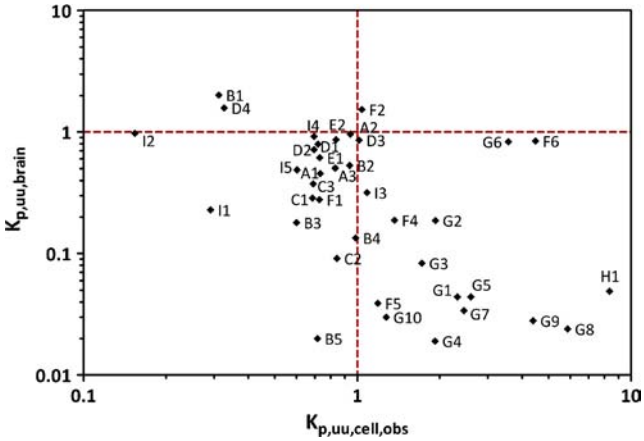

Fig. 6 Relationship between the measured unbound-drug brain ($K_{p,uu,brain}$) and intra-brain cell ($K_{p,uu,cell,obs}$) partitioning coefficients.

level as arbitrated by $K_{p,uu,brain}$ values being below 0.5 (Fig. 1). In spite of this, only ten compounds were identified as P-gp substrates using the *in vitro* LLC-MDR1 cell culture assay. This leaves 14 compounds, including five with $K_{p,uu,brain}$ below 0.1 (C2, F5, H1, G1, and G5), without efflux transporters identified that are responsible for their very high efflux. The marketed antipsychotic paliperidone (F5) is among those compounds.

Recently, the recommendation to not advance P-gp substrates as CNS drug-candidates has become prevalent within the pharmaceutical industry (8). However, each NCE has to be discussed individually and in relation to its pharmacodynamic potency, as discussed earlier. Lack of information on other drug transporters, as well as lack of sufficient knowledge on the relative importance of P-gp in the overall human neuroPK picture makes strict decisions less fruitful.

Another aspect related to transporters is the rapidly increasing evidence of expression of various influx and efflux proteins on the cell membrane of pericytes, astrocytes and

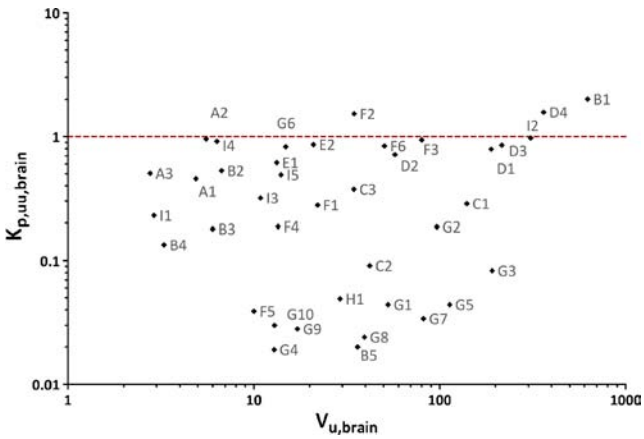

Fig. 7 Relationship between the unbound-drug brain partitioning coefficient ($K_{p,uu,brain}$) and volume of distribution of unbound-drug in brain ($V_{u,brain}$, mL g brain^{-1}).

microglia as well as their subcellular localization shown at the electron microscopy level (e.g. the nuclear envelope, cytoplasmic vesicles, Golgi complex) (34–36). This emphasizes the substantially underestimated role of cellular barriers in the intra-brain distribution of the compounds. In this regard, the estimation of $K_{p,uu,cell}$ can be a rough, but currently the only approach, for evaluation of cellular barrier function (13). Assessment of $K_{p,uu,cell}$ can be accomplished experimentally via the evaluation of $K_{p,uu,cell,obs}$ or by modeling $K_{p,uu,cell,pred}$ based on the pH partition theory.

In our dataset, it was beneficial to evaluate the neuroPK parameter $K_{p,uu,cell,obs}$ via a combination of the brain slice and brain homogenate methods, for a more profound understanding of the intra- and subcellular distribution of unbound compound. It should be noted that the numerical values obtained are an average of all cell types in the brain. The intracellular distribution is governed by quite different forces than the BBB transport. As seen in Fig. 6, the lack of correlation between $K_{p,uu,brain}$ and $K_{p,uu,cell,obs}$ is striking. For instance, several of the compounds (F5, H1, G1, G3, G4, G5, G7, G8, G9 and G10) exhibited a very low extent of BBB transport, but at the same time demonstrated a high ability to accumulate in the brain parenchymal cells. Lysosomal trapping of weak bases as well as potential involvement of active uptake transporters at the cellular barrier were found to be essential factors contributing to the accumulation of compounds in the brain parenchymal cells (25,37,38). By linking the experimentally derived $K_{p,uu,cell,obs}$ and the predicted $K_{p,uu,cell,pred}$ it is possible to convey a mechanistic elucidation of intracellular distribution, e.g. a distinction between lysosomal trapping and active uptake (Table III). For the majority of the compounds from Groups F, G and H, the sequestration into acidic organelles was found to be the main driving force of the observed intracellular accumulation (Fig. 5). Registration of higher experimental $K_{p,uu,cell,obs}$ values than those predicted by the pH partitioning model was documented for G6, G8, G9, and H2. One of the explanations of such a finding may indicate binding of compound to the lysosomal inner membrane, often associated with drug-induced phospholipidosis (39–41).

With respect to the assessment of intracerebral distribution, $V_{u,brain}$ reflects the relationship between total and unbound compound in the brain as a whole. Higher $V_{u,brain}$ values indicate a lower unbound fraction of the drug in the brain parenchyma. The overall uptake of compounds by brain slices denoted as $V_{u,brain}$ comprises mechanistically independent components such as nonspecific and specific binding, active transport, and lysosomal trapping. On the contrary, the more commonly used brain homogenate method provides information concerning nonspecific and possibly specific intracellular binding of compounds to the brain tissue, leaving other processes accountable for the intra-brain distribution uncovered. Alternatively, the correction for the pH partitioning could be

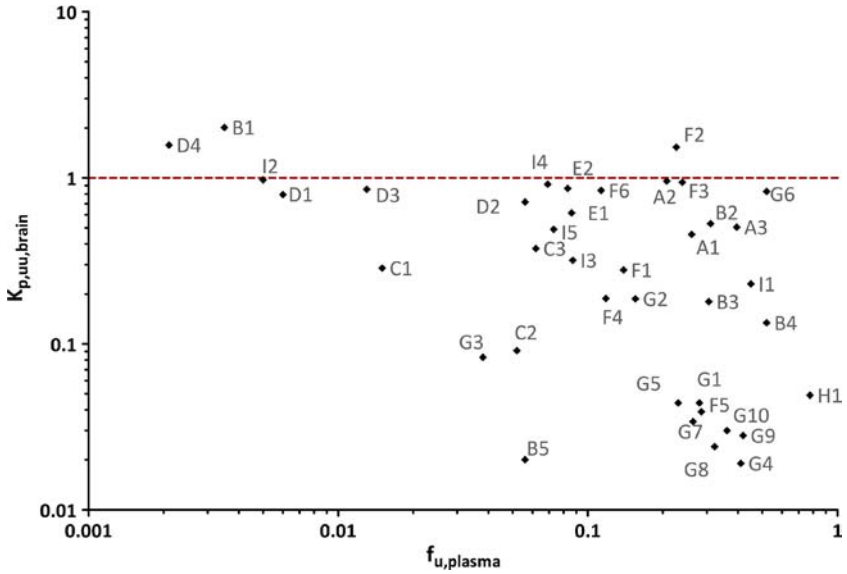

Fig. 8 Relationship between the unbound-drug brain partitioning coefficient ($K_{p,uu,brain}$) and unbound fraction of drug in plasma ($f_{u,plasma}$).

applied to $f_{u,brain}$ values with estimation of $1/f_{u,brain,corrected}$ to be used as a substitute to $V_{u,brain}$ (25). Hence, in the present dataset, a significant relationship was obtained between $V_{u,brain}$ and $1/f_{u,brain,corrected}$ ($R^2=0.79$, Fig. 4). Despite that, one has to account for the potential innate error when using $1/f_{u,brain,corrected}$ for the assessment of $K_{p,uu,brain}$ using Eq. 13.

The tendency that $1/f_{u,brain,corrected}$ overpredict $V_{u,brain}$ was observed for the current dataset. The prediction of $V_{u,brain}$ by $1/f_{u,brain,corrected}$ for the compounds B1, B5, I1, I2, and D4 was exceeding three-fold threshold. Such kind of divergence is possibly laying in the nature of the measurements used for the assessment of $V_{u,brain}$ (overall drug uptake) and $f_{u,brain}$ (mostly intracellular binding). In this regard the fact that three (B1, B5, D4) out of five compounds have extensive brain tissue binding, i.e. $f_{u,brain}$ varies from 0.0005 to 0.0009 is informative. It is known that the preparation of brain homogenates (dilution, homogenization) may modify intracellular components contributing to distribution of the drug in the brain or even bare unusual intracellular binding sites. The latter may explain very low $f_{u,brain}$ values. Besides, the weak base B1 and the neutral compounds D4, I1, and I2 are not subject to lysosomal trapping and there is no difference between $1/f_{u,brain}$ and $1/f_{u,brain,corrected}$, indicating that nonspecific binding is the main contributor to intra-brain

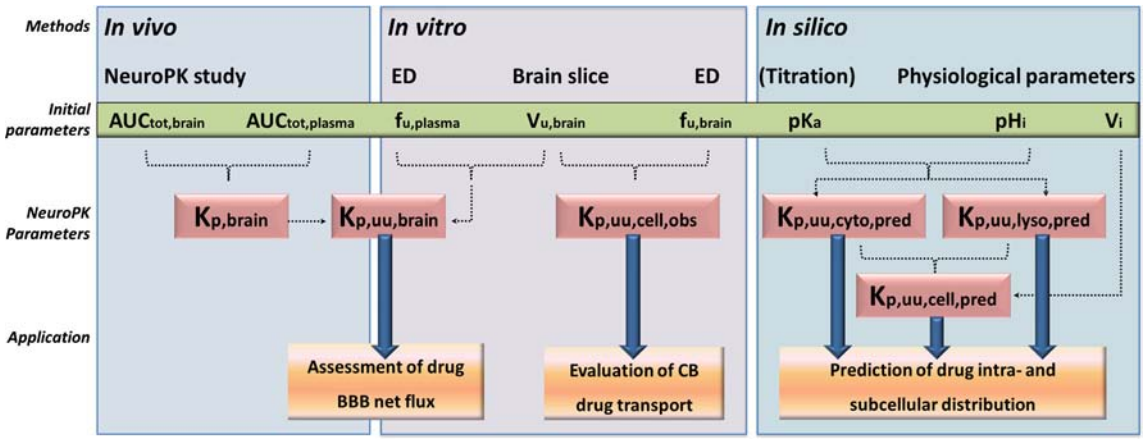

Fig. 9 Chart summarizing the combinatory mapping approach in the form of a screening toolbox for the evaluation of unbound-drug CNS exposure required for selection of effective novel neurotherapeutics and avoidance of CNS side effects for peripheral targets. The platform comprising of *in vivo*, *in vitro* and *in silico* methods is a necessity. Total drug brain and plasma exposure ($AUC_{tot,brain}$ and $AUC_{tot,plasma}$) determined in an *in vivo* neuroPK study is essential for the assessment of the brain partitioning coefficient $K_{p,brain}$. *In vitro* measurements of drug plasma and brain tissue binding properties using equilibrium dialysis (ED) and brain slice techniques are required for estimation of $K_{p,uu,brain}$ and $K_{p,uu,cell}$ neuroPK parameters. Compound-specific pK_a values (preferably measured via potentiometric titration or predicted based on physicochemical characteristics of compound) in combination with the physiological estimates of pH (pH_i) of the relevant compartments (i = plasma, ISF, cytosol or lysosomes) are used for *in silico* calculation of drug subcellular distribution, i.e. $K_{p,uu,cyto,pred}$ and $K_{p,uu,lyso,pred}$. Physiological volumes (V_i) of ISF, cytosol and lysosomes with $K_{p,uu,cyto,pred}$ and $K_{p,uu,lyso,pred}$ are used for calculation of $K_{p,uu,cell,pred}$. Assessed neuroPK parameters in conjunction with relevant pharmacodynamics readouts are recommended to be used for evaluation and selection of NCEs.

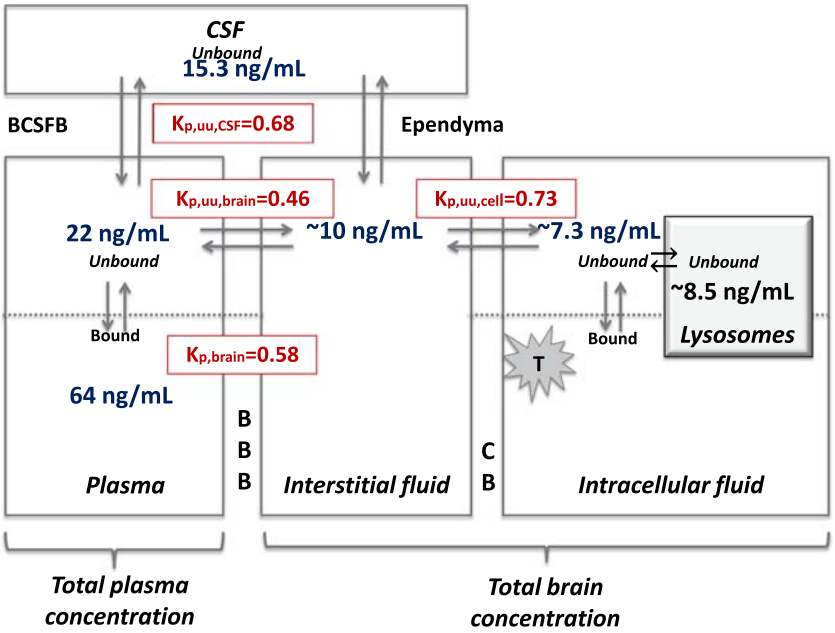

Fig. 10 Schematic representation of the distribution of A1, an NCE PDE10 inhibitor, into the different compartments (plasma, brain ISF, brain ICF, lysosomes, and CSF) involved in the disposition of drugs across the barriers (BBB, CB and BCSFB), with the resulting concentrations obtained in each compartment. T represents the intracellular localization of PDE10 enzyme. The graph was constructed using steady-state total plasma, total brain, and CSF concentrations of A1 determined in rats after a 22 h constant-rate intravenous infusion of 0.25 mg/kg h^{-1}. Using this model and given a specific plasma concentration ($f_{u,plasma,rat} = 0.26$), it is possible to estimate the target site concentration. Predicted from the pH partitioning model, $K_{p,uu,cyto,pred}$ and $K_{p,uu,lyso,pred}$ are 1.0 and 1.2, respectively (not shown in the graph). The *in vitro* IC_{50} of A1 is 14–18 ng/mL (unpublished observation). Consequently, to reach the same target-site concentration *in vivo* as the *in vitro* IC_{50}, a doubling of the dose is required. This simplified approach can be used in early drug discovery programs for establishing a link between the PK and the target engagement.

distribution. Furthermore, B1, D4, I1, and I2 exhibited very low $K_{p,uu,cell,obs}$ ranging from 0.15 to 0.33. The potential cause of such low $K_{p,uu,cell,obs}$ is not elucidated. Extensive binding to outer surface of cellular membrane of intact brain parenchymal cells may be a reason for the observed disagreement. The efflux by plasma membrane transporters should also be considered as one of the potential causes of discrepancy between the brain homogenate and brain slice methods.

The common practice by medicinal chemists to optimize novel neurotherapeutics based on $f_{u,brain}$ is profoundly incorrect, as $f_{u,brain}$ reveals nothing about the extent of BBB transport, which is the main hurdle to obtain successful compounds. The lack of any relationship between $K_{p,uu,brain}$ *vs* $V_{u,brain}$ and $K_{p,uu,brain}$ *vs* $f_{u,plasma}$ presented in Figs. 7 and 8 is evidence of that fact. Consequently, neither $f_{u,brain}$ nor $V_{u,brain}$ or $f_{u,plasma}$ should be used in isolation from BBB transport properties for the design of new neurotherapeutics. These parameters are providing information required for the assessment of the BBB transport, but without carrying any clinical relevance in them.

An alternative frequently discussed neuroPK parameter for evaluation of target-site concentration is the ratio of CSF to plasma unbound-drug concentrations $K_{p,uu,CSF}$ (42–45). However, the risk of over-predicting the unbound-drug brain concentration for compounds subjected to P-gp or BCRP transport must be considered, given that P-gp is differently expressed at the BCSFB *vs* the BBB (Supplementary Material, Figure S2) (46).

Thus far, pharmaceutical scientists have not reached a consensus on the subject of the most appropriate screening cascade for CNS-targeted substances (7,8,47–50). In this regard, the combinatory mapping approach has an important potential to be used as a screening toolbox for the assessment of CNS exposure of NCEs in the pharmaceutical industry (Fig. 9).

CONCLUSIONS

The combinatory mapping approach for assessment of brain penetration and intracellular distribution proved to be a valuable tool for evaluation of the 40 NCEs. With the rather easily-performed methods it was possible to map both the BBB and cellular barrier transport, providing quantitative knowledge supporting the decision making in regard to selection of CNS drug candidates in the drug discovery setting. Integration of neuroPK parameters with the pharmacological potency measured *in vitro* facilitates the evaluation of target engagement and further selection of NCEs. Comparison of the different neuroPK parameters also showed a lack of

correlation between them, indicating their specificity in describing mechanistically different drug transport processes.

ACKNOWLEDGMENTS AND DISCLOSURES

We express our sincere thanks to Koen Wuyts and the Early Drug Developability *in vivo* Group, Janssen Pharmaceutica for performing the neuropharmacokinetic studies and providing the $K_{p,brain}$ values. We also gratefully acknowledge the excellent assistance of Britt Jansson (Uppsala University) and Lieve Dillen, Dirk Roelant, Suzy Geerinckx (BA/DMPK, Janssen Pharmaceutica) with the bioanalysis. During the project, Irena Loryan was funded by Janssen Pharmaceutica.

REFERENCES

1. Swinney DC, Anthony J. How were new medicines discovered? Nat Rev Drug Discov. 2011;10(7):507–19.
2. Hammarlund-Udenaes M. Active-site concentrations of chemicals—are they a better predictor of effect than plasma/organ/tissue concentrations? Basic Clin Pharmacol Toxicol. 2010;106(3):215–20.
3. DiMasi JA, Feldman L, Seckler A, Wilson A. Trends in risks associated with new drug development: success rates for investigational drugs. Clin Pharmacol Ther. 2010;87(3):272–7.
4. Brunner D, Balci F, Ludvig EA. Comparative psychology and the grand challenge of drug discovery in psychiatry and neurodegeneration. Behav Processes. 2012;89(2):187–95.
5. Kaitin KI, DiMasi JA. Pharmaceutical innovation in the 21st century: new drug approvals in the first decade, 2000–2009. Clin Pharmacol Ther. 2011;89(2):183–8.
6. Ghose AK, Herbertz T, Hudkins RL, Dorsey BD, Mallamo JP. Knowledge-based, Central Nervous System (CNS) lead selection and lead optimization for CNS drug discovery. ACS Chem Neurosci. 2012;3(1):50–68.
7. Reichel A. The role of blood-brain barrier studies in the pharmaceutical industry. Curr Drug Metab. 2006;7(2):183–203.
8. Di L, Rong H, Feng B. Demystifying brain penetration in central nervous system drug discovery. J Med Chem. 2012;56:2–12.
9. Hammarlund-Udenaes M, Friden M, Syvanen S, Gupta A. On the rate and extent of drug delivery to the brain. Pharm Res. 2008;25(8):1737–50.
10. Liu X, Chen C, Smith BJ. Progress in brain penetration evaluation in drug discovery and development. J Pharmacol Exp Ther. 2008;325(2):349–56.
11. Morgan P, Van Der Graaf PH, Arrowsmith J, Feltner DE, Drummond KS, Wegner CD, *et al.* Can the flow of medicines be improved? Fundamental pharmacokinetic and pharmacological principles toward improving Phase II survival. Drug Discov Today. 2012;17(9–10):419–24.
12. Bundgaard C, Sveigaard C, Brennum LT, Stensbol TB. Associating in vitro target binding and in vivo CNS occupancy of serotonin reuptake inhibitors in rats: the role of free drug concentrations. Xenobiotica. 2012;42(3):256–65.
13. Friden M, Gupta A, Antonsson M, Bredberg U, Hammarlund-Udenaes M. In vitro methods for estimating unbound drug concentrations in the brain interstitial and intracellular fluids. Drug Metab Dispos. 2007;35(9):1711–9.
14. Gupta A, Chatelain P, Massingham R, Jonsson EN, Hammarlund-Udenaes M. Brain distribution of cetirizine enantiomers: comparison of three different tissue-to-plasma partition coefficients: K(p), K(p, u), and K(p, uu). Drug Metab Dispos. 2006;34(2):318–23.
15. Kalvass JC, Olson ER, Cassidy MP, Selley DE, Pollack GM. Pharmacokinetics and pharmacodynamics of seven opioids in P-glycoprotein-competent mice: assessment of unbound brain EC50, u and correlation of in vitro, preclinical, and clinical data. J Pharmacol Exp Ther. 2007;323(1):346–55.
16. Liu X, Vilenski O, Kwan J, Apparsundaram S, Weikert R. Unbound brain concentration determines receptor occupancy: a correlation of drug concentration and brain serotonin and dopamine reuptake transporter occupancy for eighteen compounds in rats. Drug Metab Dispos. 2009;37(7):1548–56.
17. Read KD, Braggio S. Assessing brain free fraction in early drug discovery. Expert Opin Drug Metab Toxicol. 2010;6(3):337–44.
18. Watson J, Wright S, Lucas A, Clarke KL, Viggers J, Cheetham S, *et al.* Receptor occupancy and brain free fraction. Drug Metab Dispos. 2009;37(4):753–60.
19. Kalvass JC, Maurer TS. Influence of nonspecific brain and plasma binding on CNS exposure: implications for rational drug discovery. Biopharm Drug Dispos. 2002;23(8):327–38.
20. Jeffrey P, Summerfield SG. Challenges for blood-brain barrier (BBB) screening. Xenobiotica. 2007;37(10–11):1135–51.
21. Liu X, Van Natta K, Yeo H, Vilenski O, Weller PE, Worboys PD, *et al.* Unbound drug concentration in brain homogenate and cerebral spinal fluid at steady state as a surrogate for unbound concentration in brain interstitial fluid. Drug Metab Dispos. 2009;37(4):787–93.
22. Hammarlund-Udenaes M, Bredberg U, Friden M. Methodologies to assess brain drug delivery in lead optimization. Curr Top Med Chem. 2009;9(2):148–62.
23. Friden M, Ducrozet F, Middleton B, Antonsson M, Bredberg U, Hammarlund-Udenaes M. Development of a high-throughput brain slice method for studying drug distribution in the central nervous system. Drug Metab Dispos. 2009;37(6):1226–33.
24. Loryan I, Friden M, Hammarlund-Udenaes M. The brain slice method for studying drug distribution in the CNS. Fluids Barriers CNS. 2013;10(1):6.
25. Friden M, Bergstrom F, Wan H, Rehngren M, Ahlin G, Hammarlund-Udenaes M, *et al.* Measurement of unbound drug exposure in brain: modeling of pH partitioning explains diverging results between the brain slice and brain homogenate methods. Drug Metab Dispos. 2011;39(3):353–62.
26. Boess FG, Hendrix M, van der Staay FJ, Erb C, Schreiber R, van Staveren W, *et al.* Inhibition of phosphodiesterase 2 increases neuronal cGMP, synaptic plasticity and memory performance. Neuropharmacology. 2004;47(7):1081–92.
27. May PC, Dean RA, Lowe SL, Martenyi F, Sheehan SM, Boggs LN, *et al.* Robust central reduction of amyloid-beta in humans with an orally available, non-peptidic beta-secretase inhibitor. J Neurosci. 2011;31(46):16507–16.
28. van Liempd S, Morrison D, Sysmans L, Nelis P, Mortishire-Smith R. Development and validation of a higher-throughput equilibrium dialysis assay for plasma protein binding. J Lab Autom. 2011;16(1):56–67.
29. Wan H, Rehngren M, Giordanetto F, Bergstrom F, Tunek A. High-throughput screening of drug-brain tissue binding and in silico prediction for assessment of central nervous system drug delivery. J Med Chem. 2007;50(19):4606–15.
30. Kurz H, Fichtl B. Binding of drugs to tissues. Drug Metab Rev. 1983;14(3):467–510.
31. Friden M, Ljungqvist H, Middleton B, Bredberg U, Hammarlund-Udenaes M. Improved measurement of drug exposure in the brain using drug-specific correction for residual blood. J Cereb Blood Flow Metab. 2010;30(1):150–61.
32. Nicholson C, Sykova E. Extracellular space structure revealed by diffusion analysis. Trends Neurosci. 1998;21(5):207–15.

33. Pajouhesh H, Lenz GR. Medicinal chemical properties of successful central nervous system drugs. NeuroRx. 2005;2(4):541–53.
34. Bendayan R, Ronaldson PT, Gingras D, Bendayan M. In situ localization of P-glycoprotein (ABCB1) in human and rat brain. J Histochem Cytochem. 2006;54(10):1159–67.
35. Ronaldson PT, Bendayan M, Gingras D, Piquette-Miller M, Bendayan R. Cellular localization and functional expression of P-glycoprotein in rat astrocyte cultures. J Neurochem. 2004;89(3):788–800.
36. Dallas S, Miller DS, Bendayan R. Multidrug resistance-associated proteins: expression and function in the central nervous system. Pharmacol Rev. 2006;58(2):140–61.
37. Kaufmann AM, Krise JP. Lysosomal sequestration of amine-containing drugs: analysis and therapeutic implications. J Pharm Sci. 2007;96(4):729–46.
38. Lee G, Dallas S, Hong M, Bendayan R. Drug transporters in the central nervous system: brain barriers and brain parenchyma considerations. Pharmacol Rev. 2001;53(4):569–96.
39. Duvvuri M, Krise JP. A novel assay reveals that weakly basic model compounds concentrate in lysosomes to an extent greater than pH-partitioning theory would predict. Mol Pharm. 2005;2(6):440–8.
40. Funk RS, Krise JP. Cationic amphiphilic drugs cause a marked expansion of apparent lysosomal volume: implications for an intracellular distribution-based drug interaction. Mol Pharm. 2012;9(5):1384–95.
41. Logan R, Funk RS, Axcell E, Krise JP. Drug-drug interactions involving lysosomes: mechanisms and potential clinical implications. Expert Opin Drug Metab Toxicol. 2012;8(8):943–58.
42. Friden M, Winiwarter S, Jerndal G, Bengtsson O, Wan H, Bredberg U, *et al.* Structure-brain exposure relationships in rat and human using a novel data set of unbound drug concentrations in brain interstitial and cerebrospinal fluids. J Med Chem. 2009;52(20):6233–43.
43. Lin JH. CSF as a surrogate for assessing CNS exposure: an industrial perspective. Curr Drug Metab. 2008;9(1):46–59.
44. Shen DD, Artru AA, Adkison KK. Principles and applicability of CSF sampling for the assessment of CNS drug delivery and pharmacodynamics. Adv Drug Deliv Rev. 2004;56(12):1825–57.
45. de Lange EC. Utility of CSF in translational neuroscience. J Pharmacokinet Pharmacodyn. 2013;40:315–26.
46. Gazzin S, Berengeno AL, Strazielle N, Fazzari F, Raseni A, Ostrow JD, *et al.* Modulation of Mrp1 (ABCc1) and Pgp (ABCb1) by bilirubin at the blood-CSF and blood-brain barriers in the gunn rat. PLoS ONE. 2011;6(1):e16165.
47. Reichel A. Addressing central nervous system (CNS) penetration in drug discovery: basics and implications of the evolving new concept. Chem Biodivers. 2009;6(11):2030–49.
48. Shaffer CL. Defining neuropharmacokinetic parameters in CNS drug discovery to determine cross-species pharmacologic exposure-response relationships. Annu Rep Med Chem. 2010;45:55–70.
49. Mizuno N, Niwa T, Yotsumoto Y, Sugiyama Y. Impact of drug transporter studies on drug discovery and development. Pharmacol Rev. 2003;55(3):425–61.
50. Raub TJL BS, Andrus PK, Sawada GA, Staton BA. Early preclinical evaluation of brain exposure in support of hit identification and lead optimization. Optimization of drug-like properties during lead optimization. In: Borchardt RT, Middagh CR, editors. Biotechnology: Pharmaceutical aspects series. Arlington: Am Assoc Pharm Sci Press; 2006. 5.